Eletrônica de Potência
Open Journal of Power Electronics

Received November 04, 2024; accepted February 15, 2025; Date of publication March 07, 2025.
The review of this paper was arranged by Associate Editor Hernán E. Tacca and Editor-in-Chief Heverton A. Pereira.
Digital Object Identifier http://doi.org/10.18618/REP.e202524

Power Quality Enhancement of Offshore Oil and Gas Platform with High Penetration of Wind Power and Energy Storage

Kassiane de S. Medeiros[1,*], João M. S. Callegari[1], Ayotunde A. Adeyemo[2], Elisabetta Tedeschi [2,3], Danilo I. Brandao[1]

[1]Universidade Federal de Minas Gerais, Graduate Program in Electrical Engineering, Belo Horizonte, MG, Brazil.
[2]Norwegian University of Science and Technology, Department of Electric Energy, Trondheim, Norway.
[3]University of Trento, Department of Industrial Engineering, Trento, Italy.

e-mail: kassiane@ufmg.br*, jmscallegari@ufmg.br, ayotunde.a.adeyemo@ntnu.no, elisabetta.tedeschi@ntnu.no, dibrandao@ufmg.br.
*Corresponding author

ABSTRACT This paper aims to analyze the effect of high penetration of floating offshore wind-based power generation on the power quality of a Floating Production Storage and Offloading (FPSO) power system. The paper focuses on the continuous frequency variation caused by intermittent wind power generation and an energy storage-based solution for power smoothing. A set of results simulated in MATLAB/Simulink® is shown to assess different operational scenarios of a typical Brazilian FPSO from the Mero Oil Field, powered by 109 MVA/ 87 MW from three synchronous generators, without wind power. Wind power penetration varies from 10 to 50 MW, and the effects of this variation on FPSO power quality are reported. Then, the number of gas turbine generators is reduced from 3 to 2 generators. Finally, the energy storage for power smoothing purposes is evaluated. Conclusions are drawn based on steady-state and transient voltage and frequency profiles, active and reactive power flow between loads and generation, the rate of change of frequency, and frequency nadir.

KEYWORDS Energy storage sizing, Floating production storage and offloading, Power quality, Offshore wind energy generation.

I. INTRODUCTION

A floating production storage and offloading vessel (FPSO) is an offshore oil and gas (O&G) production platform developed for deepwater (300–1500 m) and ultra-deepwater wells (beyond 1500 m). FPSO units offer a reliable and space-efficient solution for the extraction and production of deepwater oil, serving as a viable alternative to spar platforms, tension leg platforms, and semi-submersible production systems [1]. The fast-diminishing rate of discovery of new giant fields highlights the growing importance of smaller oil fields. Furthermore, for short-lived good exploration in remote marginal oil fields, building a new pipeline is cost-prohibitive [2].

The FPSO is an medium-voltage isolated power system with main energy generation composed of synchronous generators (SGs) driven by gas turbines. This system supplies different loads, such as compressors and pumps, that continuously run the O&G production. The electric energy consumption can reach tens of megawatts due to specific functions, the complexity of system composition, and the environment features [3]. Since gas turbine generators are the leading energy resource to supply the FPSO, such an application is associated with a large amount of carbon emissions [4].

Expanding oil production requires more FPSO generation capacity. However, increasing gas turbine generators is environmentally undesirable and demands significant FPSO space [5]. Renewable energy resources, specifically wind energy conversion systems (WECS), stand out as a non-polluting solution for increasing FPSO production. There are three possibilities for the allocation of wind farms: (*i*) wind turbines on the continent (i.e., onshore wind turbines), (*ii*) wind turbines on a platform exclusive to shelter generation [6], and (*iii*) offshore wind turbines. In all cases, the WECS is connected to the FPSO through an umbilical cable. The Brazilian O&G company, Petrobras, has submitted an environmental licensing request for the installation of an offshore wind farm. The project considers 178 wind turbines with 18 MW each. The ongoing regulatory discussions and large-scale projects under development show that floating offshore wind farms are a power generation option for O&G sector [7].

In recent years, many publications have dealt with offshore wind turbines, which supply electric energy to offshore O&G platforms. The authors of [8] show a strategy to add voltage and frequency control embedded in wind turbines equipped with electronic converters to improve power quality in offshore O&G installations in the North Sea. In the same

context, reference [9] shows the sensitivity analysis of the voltage and frequency variations for typical transients on an oil platform interconnected to a wind farm. The authors of [10] analyze the FPSO with a wind turbine from a low-inertia power system perspective and propose an inertia emulation control strategy to ensure stable FPSO operation. In contrast, this paper examines the effect on the FPSO power quality when connected to an offshore WECS under high penetration levels. According to [11], a high wind penetration rate is defined as exceeding 10% of the total grid power, increasing to 20% in cases where energy storage systems (ESS) are implemented. The penetration rate (PR%) is computed as $PR\% = P_{WECS}/P_{FPSO}$, i.e., the ratio between the active power from wind energy (P_{WECS}) and the total FPSO active power (P_{FPSO}), considering wind power.

The effects of high penetration of wind-based renewable energy generation are addressed by [11]–[13]. The authors of [12] evaluate the consequences of the high penetration of renewable energy on transient voltage stability, with tests from 35% to 95% penetration rates. The authors of [13] also use distinct penetration rates (13.6%, 20.6%, and 32.61%) to estimate the frequency response of a power system under high wind energy penetrations. The authors of [11] assess the effect on frequency behavior of different penetration rates (that is, 9%, 20%, 30%, 40%, and 50%) of WECS and different wind speed limits on an offshore platform. Herein, it is proposed three penetration rates: 10.3%, 36.5%, and 46.3%. In the latter scenario, carbon emission is reduced by approximately 33% compared to the base case of 3 SGs, due to the disconnection of a gas-driven SG.

Another power quality issue caused by wind power generation, equally relevant but less addressed in the literature, is continuous frequency disturbance. Grid codes tend to be more stringent for continuous frequency disturbances than transient and steady-state tolerances. ESS appear as viable solutions for frequency regulation, when needed due to heavy connection of intermittent renewables, mainly wind power generation. The frequency regulation can focus on inertia control (frequency response), primary frequency control, or power smoothing. The inertia and primary frequency control with the use of ESS [14], [15] is applied when occurs a disturbance in the frequency typically due to the shutdown of one of the SG or a large load. Power smoothing is based on correcting deviations due to the continuous intermittency of the wind power generation.

The authors of [16] evaluate the mitigation of power oscillations in a low voltage grid associated with a photovoltaic plant and connected to a battery energy storage system (BESS). They proposed a methodology that includes the combined analysis of the rainflow counting algorithm, Monte Carlo simulation, and nonlinear damage accumulation rule for battery reliability assessment. Whereas in [17], the authors have tested three power smoothing algorithms: moving average, ramp rate, and first-order low-pass filter, for generating the power reference for the ESS. The authors also analyze typical metrics for evaluating power smoothing techniques and comment on their limitations. These metrics are standard deviation, maximum variability, visual analysis, and irradiance-based metrics.

This paper is an extended version of [18], in which an ESS sizing methodology for power smoothing is included to mitigate continuous frequency disturbance. Thus, this paper employs a typical Brazilian FPSO from the Mero Oil Field, powered by 109 MVA/ 87 MW from three synchronous generators, without wind power. The results are obtained from MATLAB/Simulink® under different operational scenarios. The first parameter variation evaluated is the increase in WECS penetration (10 and 50 MW). Then, the effect of reducing the number of SG from 3 to 2 is shown. Finally, the ESS sizing and its operation for power smoothing purposes is evaluated. The conclusions are drawn based on steady-state and transient voltage and frequency profiles. The minimum power factor, the maximum rate of change of frequency (RoCoF), and the frequency nadir are also analyzed. The transient event triggered is the generation loss of 10 MW or 30 MW of wind power. The compliance with the standard is validated based on IEC 61892-1:2019 requirements [19].

This paper is structured as follows: Section II presents the FPSO electrical power system, typical frequency response after transients, relevant grid codes, and evaluated figures of merits. Section III shows the ESS methodology sizing for power smoothing. Section IV shows comparative simulation results with the proposed system scenarios. Finally, Section V discusses the conclusions regarding the power quality assessment through the proposed simulations.

II. FPSO UNIT WITH FLOATING OFFSHORE WIND

The electrical power system of a typical Brazilian FPSO from the Mero Oil Field is shown in Fig. 1. It is mainly powered by three 36.25 MVA SGs driven by gas turbines of 29 MW each and controlled as shown in [20]. The SGs are equipped with frequency and voltage slow dynamic secondary control to achieve steady-state regulation at 60 Hz and 11 kV, respectively. A total of 78.4 MW of induction motors is distributed across two electrical feeders: Topsides and Vessel. Additionally, a 10 to 50 MW WECS is integrated into the FPSO, which increases active power oscillation, and then amplifies frequency deviations. While the ESS aims at regulating frequency with a maximum deviation of 0.5% from the nominal frequency, i.e., within 59.7 Hz and 60.3 Hz, complying with IEC 61892-1:2019.

Topsides A and B are interconnected, while the circuit breaker interconnecting Vessel A and B is open. The connection circuit breakers between the Topsides and the Vessel busbars are closed. This electrical power system configuration is a radial system with selective protection. In case of a fault on a specific bus, the protection system switches off and isolates only the side with an electrical fault for the safe operation of the FPSO.

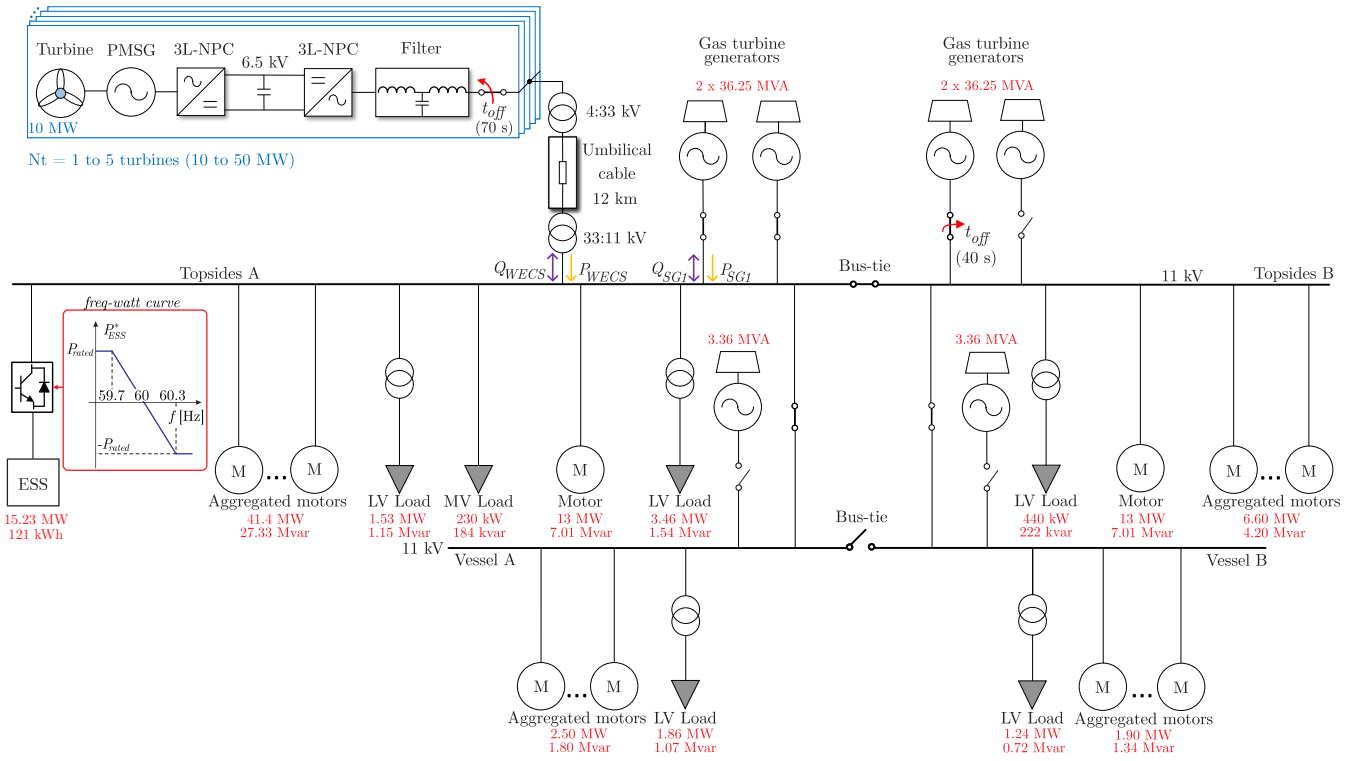

FIGURE 1. Simulated electrical power system of a typical Brazilian FPSO from Mero Oil Field.

Furthermore, 230 kW/184 kvar of one medium-voltage load and 8.53 MW/4.70 kvar of four low-voltage loads are connected through step-down transformers. The induction motors are squirrel-cage modeled with a double-cage, as in [21]. The step-down transformers are modeled based on the delta-star connection type, as shown in reference [22]. The low-voltage loads are modeled as active and reactive power (PQ) constant loads, and the medium-voltage loads are modeled as constant impedance loads. For more model details, see reference [20].

The WECS is composed of a horizontal axis wind turbine with three blades, mechanical coupling without gearbox (direct-drive), permanent magnet synchronous generator (PSMG), and an electronic back-to-back converter. The back-to-back converter is composed of a three-phase, three-level neutral point clamped (3L-NPC) rectifier, a 6.5 kV dc-bus, and a three-phase 3L-NPC inverter, controlled in grid-following mode to minimize the umbilical cable transmission losses [23]. The LCL output filter connects this converter to the umbilical cable through a 4/33 kV step-up transformer. This umbilical cable is also connected to a 33/11 kV step-down transformer to make the cable output voltage compatible with the FPSO voltage. The ESS features a cascaded H-bridge inverter with 15 submodules per phase, interfacing with the FPSO through an isolation transformer. The DC link of each low voltage submodule is equipped with a set of supercapacitors, arranged in series and parallel to meet the power and energy requirements of 15.23 MW/ 121 kWh.

Submarine umbilical cables transmit the power generated from WECS to FPSO and represent a large part of the wind farm implementation costs. In this study, the three-core cable is considered, which presents the following advantages over the single-core cable: cheaper to install; it is possible to produce the cable with integrated fiber optical cables, hence there is no need for extra operations for laying a fiber optical cable; little or no coupling to neighboring or parallel cable systems; and, reduced losses in the shield [24]. The increase in the distance between the wind farm and the FPSO means a capacitive characteristics model, higher impedance, and higher losses.

A. Frequency Response

Fig. 2 illustrates a typical grid frequency response following a generator tripping event. Immediately after the disturbance, the response is defined by the system inertia and characterized by the RoCoF. The frequency nadir is the minimum frequency reached following the disturbance. During the primary response, the governor control adds the available power to interrupt the frequency drop and reestablish the frequency balance. However, this restoration does not reach the previous nominal frequency levels. The primary response timescale is measured in seconds, generally 10 to 30 seconds. If secondary control is present, the nominal frequency is reestablished through fine adjustment of the SG governor control droop curve. The secondary control timescale typically varies from 30 seconds to several minutes or tens of minutes [25]. The SGs operate with an automatic voltage

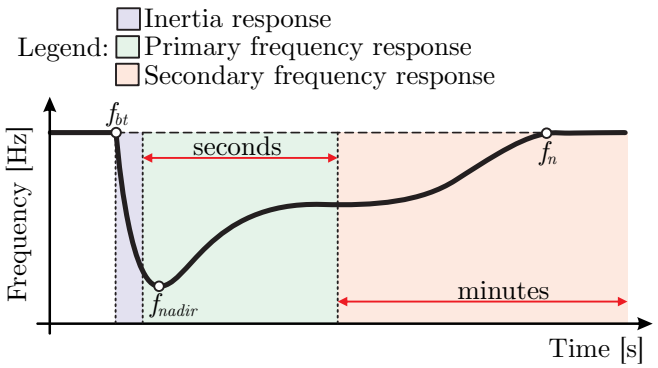

FIGURE 2. Typical frequency response following the tripping of a generator.

TABLE 1. Steady-state, transient and continuous tolerances of voltage and frequency according to IEC 61892-1:2019 [19].

	Steady-state	Transient	Continuous
Frequency	$\pm 5.0\%.f_n$	$\pm 10\%.f_n$	$0.5\%.f_n$
Voltage	$\pm 2.5\%.v_n$	+20%.v_n, -15%.v_n	-

regulator (AVR) and with governor control, the latter being the primary frequency control. Given the relatively slower time response compared to primary control, the secondary frequency control is not implemented herein without loss of generality.

B. Grid Code and Evaluated Figures of Merit

Integrating offshore WECS into an FPSO introduces continuous frequency variations due to the intermittent and turbulent nature of the wind. These continuous frequency variations are undesirable, as they lead to excessive wear and tear of SGs by repeatedly triggering their governor control to regulate active power. Standard IEC 61892-1:2019 [19] sets the maximum and minimum frequency and voltage limits during steady-state conditions and transient events. The standard also indicates a reference for the system to withstand continuous frequency variation.

Tab. 1 shows these range limits according to [19]. The frequency tolerance requirement is $\pm 5.0\%$ of nominal frequency (f_n) during steady-state conditions and $\pm 10.0\%$ of f_n for transient events. For continuous cyclic frequency variation, the IEC 61892-1:2019 sets a tolerance of 0.5% of the nominal frequency. Thus, it is essential to smooth the WECS power fluctuation using an ESS. The voltage tolerance requirement is $\pm 2.5\%$ of nominal voltage (v_n) during steady-state conditions, and -15% of v_n to +20% of v_n for transient events.

Power quality issues caused by WECS connection to FPSO are quantified in this paper using the following figures of merit:

1) Voltage variation: $\Delta V = V_{max} - V_{min}$.
2) Frequency variation: $\Delta f = f_{max} - f_{min}$.
3) Minimum power factor: min (PF) = $min(P/|S|)$.
4) Maximum RoCoF: max$|RoCoF| = max|df/dt|$.
5) Frequency nadir variation: $\Delta f_{nadir} = f_{bt} - f_{nadir}$.

The minimum and maximum values of 1), 2), and 3) are considered at the Topsides busbar within an evaluated time window during steady-state. P and S are the active and apparent power provided by an SG. For transient evaluation, 4) and 5) are considered. RoCoF is computed using an attenuated 100 kHz bandwidth low-pass filter followed by a derivative function. The frequency nadir variation (Δf_{nadir}) is defined as the variation between the frequency before the transient event (f_{bt}) and the frequency nadir, f_{nadir}. Herein, Δf_{nadir} is used instead of f_{nadir} due to the lack of secondary control implemented on the SGs.

III. SIZING OF ENERGY STORAGE FOR POWER SMOOTHING

Traditional power smoothing strategies for WECS often involve operating the system outside of its maximum power point (MPP). This approach reduces power fluctuations, but also leads to a loss in power generation. These methods, as discussed in [26]–[28], prioritize smoothing power variations at the cost of reduced energy production, which lowers the overall efficiency of the system. To prevent a reduction in the power generated by WECS, an alternative to maintaining the system at its MPP while simultaneously achieving the power and frequency smoothing objective is the integration of ESS into the FPSO platform, as implemented herein. Essentially, the difference between the frequency smoothing strategies embedded in the ESS is based on the way the active power reference is generated to be injected or absorbed. For this offshore FPSO application, the autonomous freq-watt strategy is adopted as it eliminates the need for additional sensors. It is worth highlighting that the freq-watt strategy is not a contribution of this paper. The focus is on the methodology for sizing the ESS to provide power smoothing.

The challenge of smoothing the WECS power fluctuations using an ESS depends on determining the appropriate size of the ESS, including its power and energy ratings. The swing equation, which describes the rotor dynamics of SGs, has been implemented to represent the frequency behavior of the FPSO power system under significant electrical penetration disturbances from the WECS, as in [29]:

$$\frac{2H}{\omega_m} \cdot \frac{d^2\delta}{dt^2} = P_m + P_{ess} - P_e, \tag{1}$$

where δ is the rotor angular position according to the position of the synchronously rotating magnetic field, H is the inertia constant, ω_m is the synchronous speed of the machine magnetic field, P_m is the mechanical power, P_{ess} is the ESS power and P_e is the electrical power or load on the SGs. The authors of [30] show that the simplified model based on (1) can produce a frequency response that closely resembles that of the detailed model with the voltage dynamics incorporation. Also, the detailed model can be particularly time-consuming when sizing the ESS using a

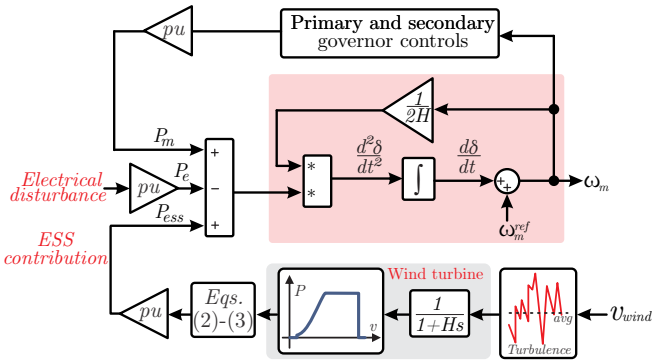

FIGURE 3. Block diagram of FPSO frequency response simulation.

full day of data, so it is often avoided. The block diagram that calculates the FPSO frequency response is shown in Fig. 3.

The power contribution of the ESS for power smoothing is closely linked to the WECS power intermittency. Fig. 3 shows the algorithm employed to generate turbulence in wind speed based on a specified average wind speed. The turbine inertia constant is considered to evaluate how variations in wind speed influence the WECS output power. The smoothing power of the ESS is determined by calculating a moving average of the WECS power over a 5-minute window. The following equations outline the method for calculating the smoothing power:

$$P_{wf\_avg}[n] = \frac{1}{N}\sum_{k=0}^{N-1} P_{wf}[n-k] \tag{2}$$

$$P_{ess}[n] = P_{wf\_avg}[n] - P_{wf}[n], \tag{3}$$

where $P_{wf\_avg}[n]$ is the WECS average power for the last 5 minutes, n is the sample index, N is the total number of samples within the 5-minute window depending on the sampling time, $P_{wf}[n-k]$ is the actual WECS power at a specific point in the past indicated by the sample number $n-k$, P_{ess} is the smoothing power that needs to be supplied by the ESS, and $P_{wf}[n]$ is the wind farm power in the current sample n.

The data for the WECS is presented in Table 2, with the rated mechanical power chosen as the base power for calculating the per unit values. The wind turbulence is initially simulated using the data from Table 2, which reveals that the wind speed oscillates by an average of ± 2 m/s around the mean wind speed. This ± 2 m/s variation is then applied to set the average wind speed that results in the maximum change in WECS power and the maximum energy rating. By examining the wind speed range of 4-11 m/s, an average wind speed of 9 m/s is identified as requiring both the maximum power rating and maximum energy rating.

Five wind turbines (i.e., N_t = 5) are utilized, with each WECS assumed to supply a maximum of 10 MW despite a rated power of 11 MW. This ensures consistency throughout the analysis of a 50 MW wind farm. The model is simulated

TABLE 2. WECS parameters.

Parameter	Value
Rated mechanical power	11 MW
Rated mechanical speed	10 rpm
Minimum wind speed	4 m/s
Rated wind speed	11 m/s
Maximum wind speed	25 m/s
Equivalent moment of inertia	7.3 $\times 10^7$ kgm^2
Blade diameter	194 m
Turbulence intensity	6 %
Number of turbines	5
WECS curve	[0, 4, 5, 6, 7, 8, 9, 10, 11, 25, 30] m/s
v_{wind} (m/s) x P (pu)	[0, 0, 0.095, 0.16, 0.26, 0.38, 0.55, 0.75, 1, 1, 0] pu

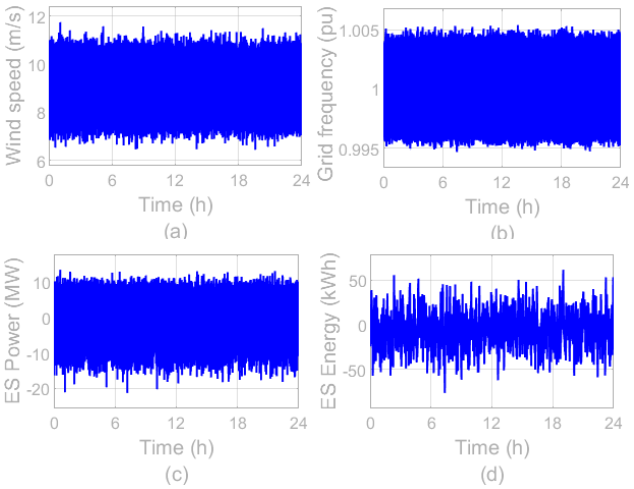

FIGURE 4. Results of the ESS sizing using the 9 m/s average wind speed.

over 86,400 seconds (i.e., one day), and the resulting wind speed profile, grid frequency, ESS power, and ESS energy are shown in Fig. 4. As shown in Fig. 4 (a), the wind speed fluctuates by 2 m/s around the average. Fig. 4(b) shows that the grid frequency remains within $\pm 0.5\%$. The WECS maximum power output in Fig. 4(c) is -21.3 MW, while the required energy rating, as shown in Fig. 4(d), is 121 kWh (i.e., the maximum variation of energy). Moreover, the ESS power rating can be further minimized since maintaining a maximum continuous frequency variation of 0.5% is sufficient. The approach for determining the optimal power rating is detailed in the flow chart in Fig. 5.

The region reduction iterative algorithm (RRIA) starts by setting the lower bound for the solution region, $\chi_{min}(k)$, to zero and the upper bound for the solution region, $\chi_{max}(k)$, to a reasonably high value that satisfies the condition of the algorithm for the first iteration k=1. For k=1, $\chi_{max}(k)$ is set to the preliminary power rating of 21.3 MW, as obtained from previous results. Then, the ESS rating, $P_{ess} = \frac{\chi_{min}(k)+\chi_{max}(k)}{2}$, is determined. The difference between the upper bound and lower bound, $\varepsilon(k)$, is also computed. The parameter ε_o is the threshold for stopping the iteration and is set to 0.01 MW herein. $\mathcal{F}^p$ denotes the maximum number of times the FPSO grid frequency may exceed 0.5% due to

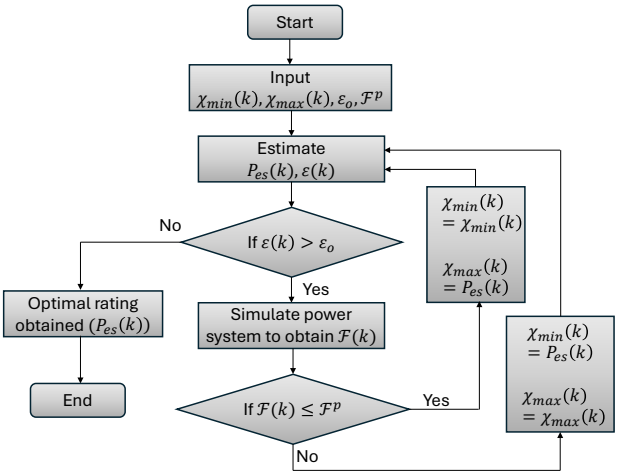

FIGURE 5. Region reduction iterative algorithm for determining the optimal ESS power rating.

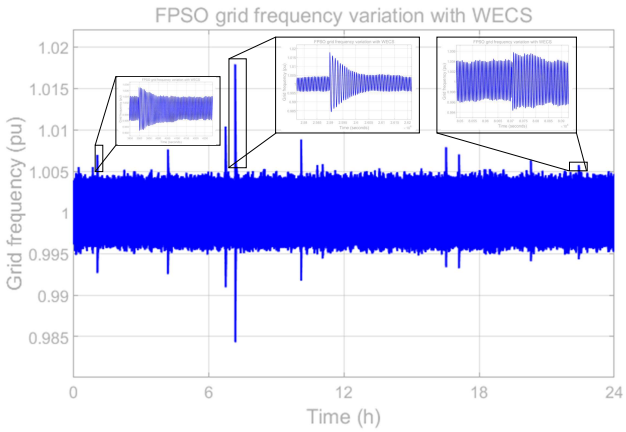

FIGURE 6. FPSO grid frequency with a reduced ESS rating of 15.23 MW/ 121 kWh obtained from the RRIA.

variations in WECS power. In this paper, $\mathcal{F}^p$ is set to 48, implying that the FPSO grid frequency is allowed to exceed the 0.5% threshold on average once every 30 minutes. This interval is sufficiently large to be considered a transient event rather than a continuous frequency variation.

During the first iteration, the RRIA checks whether $\varepsilon(k) > \varepsilon_o$. If this condition is satisfied, the system is simulated with the calculated ESS power rating, P_{ess}. $\mathcal{F}(k)$ is the number of times the frequency exceeded 0.5% during a day of simulation. If $\mathcal{F}(k) \leq \mathcal{F}^p$, $\chi_{min}(k)$ is set to $\chi_{min}(k)$ and $\chi_{max}(k)$ is set to $P_{ess}(k)$. Conversely, if $\mathcal{F}(k) > \mathcal{F}^p$, $\chi_{min}(k)$ is updated to $P_{ess}(k)$ and $\chi_{max}(k)$ remains unchanged. In subsequent iterations, $P_{ess}(k)$ and $\varepsilon(k)$ are recalculated, and the RRIA again checks whether $\varepsilon(k) > \varepsilon_o$. If this condition holds, the system is simulated once more. The algorithm continues until $\varepsilon(k) < \varepsilon_o$, at which point the iteration stops, and the last ESS power rating $P_{ess}(k)$ is selected as the optimal rating. Running the RRIA algorithm provided a reduced power of 15.23 MW. The FPSO grid frequency with this power rating and an energy rating of 121 kWh is shown in Fig. 6.

It can be seen from Fig. 6 that the FPSO grid frequency is limited to 0.5% continuously. The three frequency deviations that exceeding $\pm 0.5\%$ are highlighted in Fig. 6, which are essentially considered transient events. The frequency of the system takes approximately 100 seconds to recover. As shown in Fig. 6, a continuous frequency deviation of $\pm 0.4\%$ persists due to ongoing variations in wind speed. After each transient event where the deviation exceeds $\pm 0.5\%$, the frequency stabilizes to its normal operating condition of $\pm 0.4\%$ in approximately 100 seconds. Since these deviations beyond $\pm 0.5\%$ are short-lived and last no more than 100 seconds, they are classified as transient events.

With the ESS power and energy ratings established, attention turns to the practical implementation of these ratings. For this, the supercapacitor appears to be the best current mature technology option. A 144 V, 62.5 F Eaton supercapacitor module, rated at 420 kW and 180 Wh, is used as the base unit in this paper [31]. It is worth noting that not all of the stored energy in the supercapacitor can be utilized due to significant voltage variations during operation. Therefore, it is practical to limit the discharge to 50% of its rated voltage, allowing for the extraction of 75% of the total stored energy. To meet the required ESS ratings, 900 units of the base module are configured in a series-parallel arrangement, consisting of 90 parallel connections and 10 series connections. This configuration results in a total rated voltage of 1440 V, a usable energy capacity of 121.5 kWh, and a maximum power output of 37.8 MW. However, only 15.23 MW is necessary from the supercapacitor bank, meaning the maximum capacity of 37.8 MW will not be fully utilized.

Supercapacitors are one of many energy storage technologies that can be utilized for this application. In wind power smoothing applications, energy storage systems must be able to deliver high charge/discharge rate capabilities (C-rates) to respond quickly to fluctuations in WECS. Although solid-state batteries offer significant advantages, such as high energy density [32] and improved safety over conventional lithium-ion batteries [33], they generally exhibit lower C-rate capabilities (around 1 to 2C). This limitation makes them less suitable for managing the high-frequency charge-discharge cycles needed to smooth transient wind power fluctuations. Flywheels, in contrast, excel in high-power, short-duration applications [34], offering instantaneous power with C-rates exceeding 100C. However, their relatively limited energy storage capacity restricts their effectiveness in sustaining power smoothing over extended periods. Lithium-ion capacitors (LICs) offer a middle ground with C-rates typically 10 to 50C, allowing them to handle rapid fluctuations and moderate energy requirements efficiently [35]. Nevertheless, even these alternatives fall short of supercapacitors, which boast

TABLE 3. Configurations of the case study.

Case	Active wind power	SGs	Umbilical cable	ESS
1	10 MW x 50 MW	3 SG	12 km	No
2	50 MW	3 SG x 2 SG	150km	No
3	50 MW	2 SG	12 km	Yes

extraordinarily high C-rates (up to 10,000C) and unparalleled power density [31], making them the best suited to handle wind power variability. Although supercapacitors are ideal for handling short-term transients, their low energy density limits their application in scenarios where both high energy capacity and rapid response are required, necessitating a hybrid or complementary system for optimal performance [29].

IV. SIMULATION RESULTS

The models of each part of the system are simulated in MATLAB/Simulink® with a step simulation of 100 μs using a discrete solver. The results are split into three case studies, as shown in Tab. 3. *Case 1* analyzes the consequences of increasing the offshore WECS active power, while *Case 2* evaluates the results outage of an SG, and *Case 3* analyzes the power smoothing effects with the ESS employment. For the first and second case studies, the steady-state figures of merit are computed between 50 and 69 s, while the transient event is considered within the 70 - 74 s time window. The third case study considers only steady-state, with results showed during 60 - 250 s. Only the result of SG_1 is shown since the droop-based control performs accurate power-sharing among SGs.

A. Case 1: Increase of the Floating Offshore Wind Active Power

Fig. 7 (a) shows the active and reactive power in SG_1 (P_{SG1} and Q_{SG1}), and (b) the active and reactive power in WECS (P_{WECS} and Q_{WECS}). The simulation results with 10 MW (Nt = 1) or 50 MW (Nt = 5) of WECS show that the active power in SG_1 decreases when compared to the system without (w/o) wind generation, representing a relief in SG operation. The number of turbines affects the umbilical cable parameters and results in increased injection of reactive power by the umbilical cable into the FPSO system. After the transient event (shutdown of one turbine at t = 70 s), WECS reactive power is adjusted to minimize losses in the umbilical cable.

The increase in wind energy generation from 10 to 50 MW results in a more disturbed FPSO voltage and frequency - see Fig. 7 (c). Figs. 7 (c)-(d) and Tab. 4 express this aggravation of voltage and frequency variation, i.e., 122% and 230%, respectively. Nonetheless, the voltage and frequency limits shown in Tab. 1 [19] are not reached. The minimum power factor is influenced by both the reactive powers exchanged and the active powers available in the system. It also shows deterioration, with a reduction of 17%.

The figures of merit for evaluating the system behavior during transient events, max$|RoCoF|$ and Δf_{nadir}, are not negatively affected by the increase in wind generation. The maximum RoCoF presents a reduction of 2.3% while, the frequency nadir variation shows a reduction of 3.1%. The results show that the increased disturbance, due to increased wind energy penetration, is more significant in steady-state conditions.

B. Case 2: Number of Gas Turbine Generators Reduction

Since the WECS and SGs are current- and voltage-controlled, respectively, the SGs complement the power demand from the loads subtracted from the WECS injected power. With the shutdown of one SG, the remaining two generators operate with increased active power, from 20 MW to 29 MW each, which is the SG maximum active power available - see Figs. 7 (h) and (i).

Due to the slow dynamics of the governor control, the frequency oscillates following WECS active power fluctuation (P_{WECS}), see Fig. 7 (k). Due to the AVR slow dynamics and the power coupling caused by the FPSO line impedances, with the WECS penetration, the Topsides voltage also fluctuates, see Fig. 7 (j). Tab. 4 shows that during the shutdown of an SG, all figures of merit deteriorate: voltage variation increases by 127%, frequency variation increases by 38%, maximum RoCoF increases by 41%, frequency nadir variation increases by 37%, and minimum PF decreases by 1.7%. During the transient events (i.e., N_t from 5 to 2) and within the steady-state operation, voltage and frequency values have not reached the limits shown in Tab. 1 [19].

C. Case 3: Frequency Response Enhancement with Energy Storage System

Fig. 8 shows the simulation results of the FPSO under two operational scenarios: (i) without ESS and (ii) with 15.23 MW/ 121 kWh ESS for wind power smoothing, and consequently frequency support. A 50 MW WECS penetration and two operational SGs are simulated in both scenarios. No transition is enabled in Fig. 8. The focus is on power smoothing by the ESS to reduce continuous SG frequency fluctuations, keeping it within the 60 Hz $\pm$0.5% limits.

Fig. 8 (a) shows the frequency fluctuations caused by the intermittent WECS active power, both with and without the ESS installed. Within the simulated 60 to 250 seconds (i.e., less than 5 minutes), there are 20 violations of the continuous frequency variation limits of $\pm$0.5% (i.e., specified by the IEC 61892-1:2019) when the ESS is not employed. In contrast, there are no limit violations when the ESS is used during this period. Fig. 8 (b) shows the active power measured at the SG output terminals, with and without ESS. The high dP/dt observed in P_{SG1} without the ESS leads to continuous frequency fluctuations that exceed regulatory limits, resulting from the limited bandwidth of the primary and secondary governor controls. The smoothing of SG

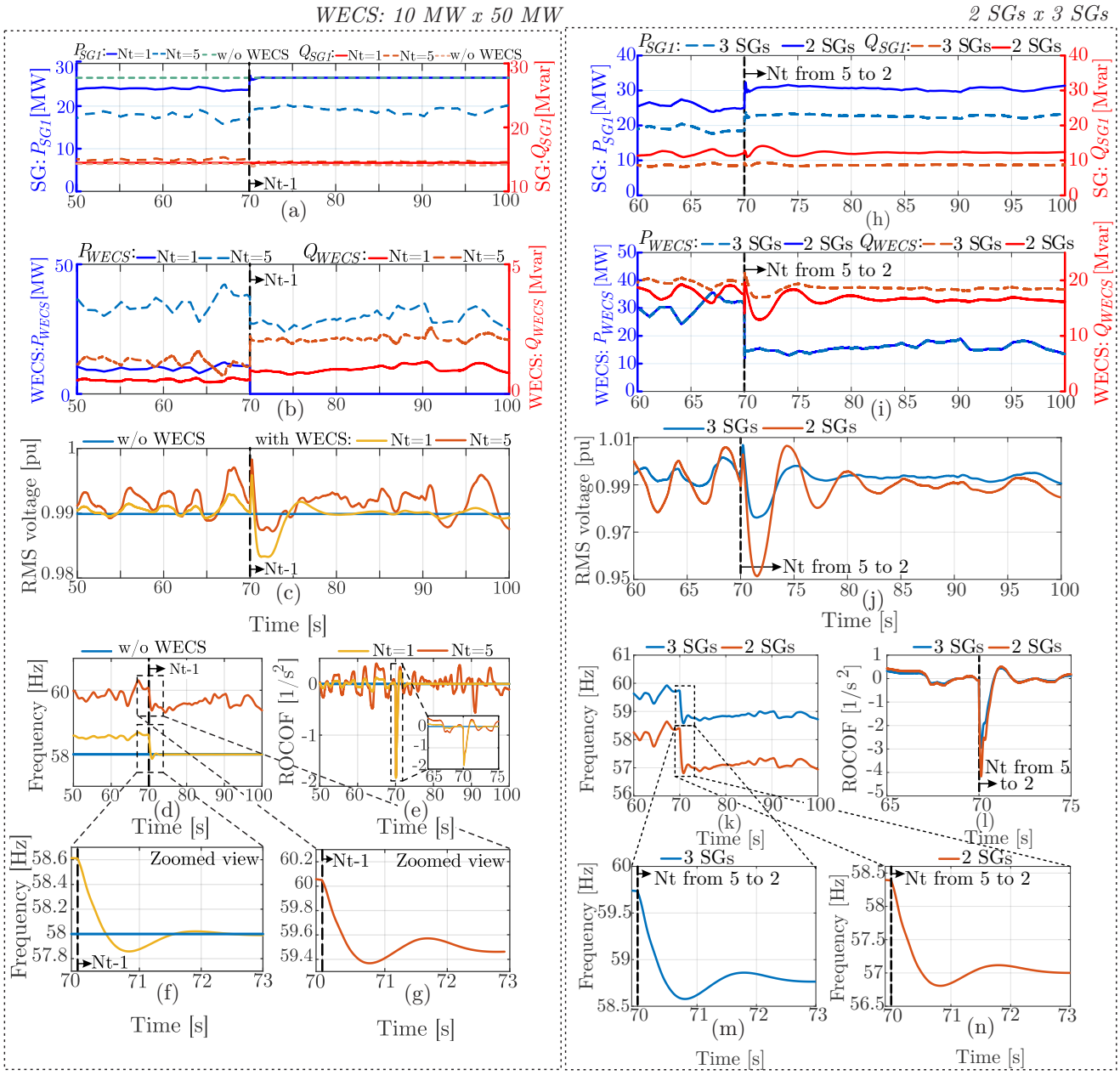

FIGURE 7. Simulated results considering 10 MW x 50 MW of WECS. Active and reactive power at (a) SG_1, (b) WECS. (c) Topsides RMS voltage. (d) FPSO frequency. (e) RoCoF. (f) Zoomed view frequency with 10 MW of WECS. (g) Zoomed view frequency with 50 MW of WECS. Simulated results considering 3 SGs x 2 SGs. Active and reactive power at (h) SG_1, (i) WECS. (j) Topsides RMS voltage. (k) FPSO frequency. (l) RoCoF. (m) Zoomed view frequency with 3 SGs. (n) Zoomed view frequency with 2 SGs.

power transitions (i.e., reduced dP/dt) after installation of the ESS allows sufficient governor control bandwidth to reduce frequency fluctuations within acceptable limits - see Fig. 8 (a).

Fig. 8 (c) shows the charging power (i.e., $P_{ESS} > 0$) and discharging power (i.e., $P_{ESS} < 0$) at the ESS output terminals. The supercapacitors corresponding percentage of energy and voltage are shown in Fig. 8 (d). An energy balancing strategy ensures the ESS is available for frequency support. This strategy maintains the stored energy of supercapacitors at 50% (on average) when the frequency is within acceptable limits. Therefore, the ESS stores excess energy during periods of high WECS generation and releases it during low WECS generation, smoothing the power output at the SGs. As shown in Fig. 8, this effectively stabilizes the frequency and keeps frequency deviations within acceptable operational limits, which enhances the reliability and resilience of the FPSO power system.

Finally, to compare with case studies 1 and 2, Table 4 highlights the enhancement in the evaluated steady-state

TABLE 4. Numerical results for the study of cases.

Configuration					Steady-state			Transient-state	
Case	P_{WECS} (MW)	SGs	l_{umb} (km)	ESS	ΔV (pu)	Δf (Hz)	min(PF)	max$\lvert RoCoF\rvert$ ($1/s^2$)	Δf_{nadir} (Hz)
1	10	3	12	-	0.0037	0.2442	0.8487	1.8349	0.7543
	50	3	12	-	0.0082	0.8059	0.7075	1.7933	0.7309
Percentage increase: [(final value - initial value) / initial value] x 100%					+ 122%	+ 230%	- 17%	- 2.3%	- 3.1 %
2	50	3	150	-	0.0121	0.6448	0.8782	2.9471	1.1622
	50	2	150	-	0.0275	0.8886	0.8637	4.1679	1.5899
Percentage increase: [(final value - initial value) / initial value] x 100%					+ 127%	+ 38%	- 1.7%	+ 41%	+ 37%
3	50	2	12	-	0.0295	1.1959	0.6442	-	-
	50	2	12	15.23 MW/ 121 kWh	0.0181	0.5283	0.6475	-	-
Percentage increase: [(final value - initial value) / initial value] x 100%					-39%	-56%	+0.5%	-	-

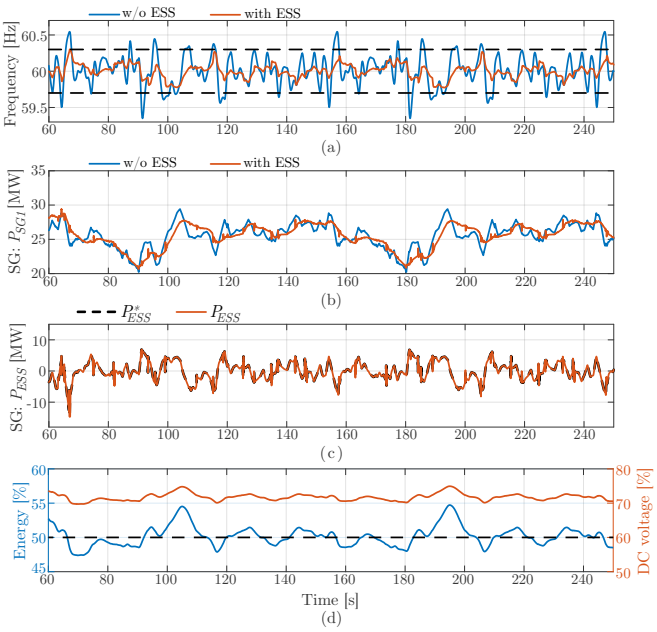

FIGURE 8. Simulated results for the FPSO without an ESS and with a 15.23 MW/121 kWh ESS: (a) frequency; (b) active power at the SG terminals; (c) active power at the ESS terminals; and (d) energy and voltage of the supercapacitors within the ESS.

figures of merit. Voltage variation reduces by 39%, frequency deviation reduces by 56%, and the minimum PF increases by 0.5%.

V. CONCLUSIONS

This paper analyzed power quality parameters related to voltage and frequency in steady-state and transient conditions under different operational scenarios in an FPSO application. Simulation results demonstrated that for the analyzed cases, even the most critical one, i.e., the one with the smallest system inertia with two synchronous generators and 50 MW of wind power, the steady-state and transient voltage and frequency variations remained within the tolerance values established by IEC 61892-1:2019. Except to the continuous frequency variation that exceeded the allowable limits established by IEC 61892-1:2019. The inclusion of an sized energy storage system regulated the continuous frequency variation within acceptable limits.

When wind energy integration to the FPSO was increased from 10 MW to 50 MW, representing 36.5% wind penetration, the results showed a substantial rise in voltage variation (122%) and an even more pronounced increase in frequency variation (230%) during steady-state conditions, with frequency deviations being particularly significant. The figures of merit for transient events did not show notable changes, indicating that with higher wind penetration, frequency stability should become a priority in developing solutions for the FPSO electrical system.

Another scenario involved shutting down one of the synchronous generators, increasing wind penetration to 46.3% and reducing carbon emissions by 33%. This situation resulted in greater disturbances in all the figures of merit. Tackling these disturbances will require targeted solutions for both steady-state and transient conditions, which proves more challenging than other scenarios.

Finally, the use of an ESS to mitigate frequency variations caused by wind power intermittency was evaluated. The sizing of a 15.23 MW/121 kWh ESS limited the continuous frequency variation within $\pm 0.5\%$, in accordance with IEC 61892-1:2019. The quantitative assessment of these disturbances provides valuable insights for enhancing FPSO system electrification and improving generation sustainability by reducing carbon emissions.

ACKNOWLEDGMENT

This paper was carried out partly by the Coordination for the Improvement of Higher Education Personnel - Brazil (CAPES) through the Academic Excellence Program (PROEX), partly by the National Council for Scientific and Technological Development– Brazil (CNPq), grant 150671/2024-5, partly by the Minas Gerais Research Funding Foundation (FAPEMIG), grants: BPD-00718-22, APQ-02216-23 and APQ-05085-23, and partly by the program PETROMAKS2 of the Research Council of Norway within the project “Smart Platform” with grant number 308735.

AUTHOR'S CONTRIBUTIONS

K. S. MEDEIROS: Conceptualization, Data Curation, Formal Analysis, Investigation, Methodology, Software, Validation, Visualization, Writing – Original Draft. **J. M. S. CALLEGARI**: Conceptualization, Data Curation, Formal Analysis, Investigation, Methodology, Software, Supervision, Validation, Visualization, Writing – Review & Editing. **A. A. ADEYEMO**: Conceptualization, Data Curation, Formal Analysis, Investigation, Methodology, Software, Supervision, Validation, Writing – Review & Editing. **E. TEDESCHI**: Conceptualization, Funding Acquisition, Project Administration, Resources, Supervision, Visualization, Writing – Review & Editing. **D. I. BRANDAO**: Conceptualization, Formal Analysis, Funding Acquisition, Methodology, Project Administration, Resources, Supervision, Visualization, , Writing – Review & Editing.

PLAGIARISM POLICY

This article was submitted to the similarity system provided by Crossref and powered by iThenticate – Similarity Check.

REFERENCES

[1] R. Brown, "FPSO: lessons learned", *IEEE Industry Applications Magazine*, vol. 10, no. 2, pp. 18–23, 2004, doi:10.1109/MIA.2004.1270797.

[2] "Energy optimization of an FPSO operating in the Brazilian Pre-salt region", *Energy*, vol. 164, pp. 390–399, 2018, doi:https://doi.org/10.1016/j.energy.2018.08.203.

[3] T.-V. Nguyen, S. de Oliveira Júnior, "Life performance of oil and gas platforms for various production profiles and feed compositions", *Energy*, vol. 161, pp. 583–594, 2018, doi:https://doi.org/10.1016/j.energy.2018.07.121.

[4] Z. Li, H. Zhang, J. Meng, Y. Long, Y. Yan, M. Li, Z. Huang, Y. Liang, "Reducing carbon footprint of deep-sea oil and gas field exploitation by optimization for Floating Production Storage and Offloading", *Applied Energy*, vol. 261, p. 114398, 2020, doi:https://doi.org/10.1016/j.apenergy.2019.114398.

[5] X. Zhou, Y. Liang, S. Xin, P. Di, Y. Yan, H. Zhang, "A MINLP model for the optimal waterflooding strategy and operation control of surface waterflooding pipeline network considering reservoir characteristics", *Computers & Chemical Engineering*, vol. 129, p. 106512, 2019, doi:https://doi.org/10.1016/j.compchemeng.2019.106512.

[6] L. F. N. Lourenço, D. F. Pereira, R. M. Monaro, M. B. C. Salles, R. M. P. Rosa, "Assessment of an Isolated Offshore Power Grid Based on the Power Hub Concept for Pre-Salt Oil and Gas Production", *IEEE Access*, vol. 10, pp. 87671–87680, 2022, doi:10.1109/ACCESS.2022.3199761.

[7] D. Zaparolli, "Usinas eólicas em alto-mar podem fornecer eletricidade para plataformas de petróleo", Accessed on January 31, 2025, Revista Pesquisa FAPESP, ed. 334, 2023, URL: https://revistapesquisa.fapesp.br/usinas-eolicas-em-alto-mar-podem-fornecer-eletricidade-para-plataformas-de-petroleo.

[8] A. R. Årdal, T. Undeland, K. Sharifabadi, "Voltage and Frequency Control in Offshore Wind Turbines Connected to Isolated Oil Platform Power Systems", *Energy Procedia*, vol. 24, pp. 229–236, 2012, doi:https://doi.org/10.1016/j.egypro.2012.06.104.

[9] A. R. Årdal, S. D'Arco, R. E. Torres-Olguin, T. Undeland, K. Shrarifabadi, "Parametric sensitivity of transients in an islanded system with an offshore wind farm connected to an oil platform", *in Proceedings of the 2011 14th European Conference on Power Electronics and Applications*, pp. 1–10, 2011.

[10] A. R. Årdal, K. Sharifabadi, O. Bergvoll, V. Berge, "Challenges with integration and operation of offshore oil & gas platforms connected to an offshore wind power plant", *in 2014 Petroleum and Chemical Industry Conference Europe*, pp. 1–9, 2014, doi:10.1109/PCICEurope.2014.6900054.

[11] Q. Yu, Y. Liu, Z. Jiang, L. Li, Y. Zhang, M. Guo, "Study of offshore wind power penetration rate in gas turbine generator platform power grid", *Energy Reports*, vol. 7, pp. 141–146, 2021, doi:https://doi.org/10.1016/j.egyr.2021.02.011.

[12] S. Niu, Z. Zhang, X. Ke, G. Zhang, C. Huo, B. Qin, "Impact of renewable energy penetration rate on power system transient voltage stability", *Energy Reports*, vol. 8, pp. 487–492, 2022, doi:https://doi.org/10.1016/j.egyr.2021.11.160.

[13] J. D. Lara-Jimenez, J. M. Ramirez, "Inertial frequency response estimation in a power system with high wind energy penetration", *in 2015 IEEE Eindhoven PowerTech*, pp. 1–6, 2015, doi:10.1109/PTC.2015.7232516.

[14] V. Knap, S. K. Chaudhary, D.-I. Stroe, M. Swierczynski, B.-I. Craciun, R. Teodorescu, "Sizing of an Energy Storage System for Grid Inertial Response and Primary Frequency Reserve", *IEEE Transactions on Power Systems*, vol. 31, no. 5, pp. 3447–3456, 2016, doi:10.1109/TPWRS.2015.2503565.

[15] A. A. Adeyemo, E. Tedeschi, "Sizing of Energy Storage for Virtual Inertia Emulation and Primary Frequency Control in Low-Inertia Systems", *in 2022 5th International Conference on Power and Energy Applications (ICPEA)*, pp. 480–486, 2022, doi:10.1109/ICPEA56363.2022.10052579.

[16] W. Amorim, A. Cupertino, V. Mendes, R. Oliveira de Sousa, R. de Barros, H. Pereira, "On Reliability Assessment of a Battery Energy Storage Systems Supporting PV Plants", , 11 2023, doi:10.1109/SPEC56436.2023.10408077.

[17] R. M. de Souza, F. J. P. Ferreira, A. S. Neto, R. C. Neto, F. A. S. Neves, J. F. C. Castro, "An Analysis of the Limitations of Power Smoothing Metrics and Future Perspectives for Their Evolution in the Context of BESS-Based Systems", *Eletrônica de Potência*, vol. 29, p. e202423, Aug. 2024, doi:10.18618/REP.2005.2.017021.

[18] K. d. S. Medeiros, J. M. S. Callegari, L. F. da Rocha, D. I. Brandao, "Power Quality Assessment of Oil and Gas Platform with High Penetration of Floating Offshore Wind Power", *in 2023 IEEE 8th Southern Power Electronics Conference and 17th Brazilian Power Electronics Conference (SPEC/COBEP)*, pp. 1–7, 2023, doi:10.1109/SPEC56436.2023.10408371.

[19] IEC, "Mobile and fixed offshore units - Electrical installations - Part 1: General requirements and conditions", *IEC 61892-1:2019*, 2019.

[20] H. M. A. Antunes, D. I. Brandao, V. H. M. Biajo, M. H. S. Alves, F. S. Oliveira, S. M. Silva, "Floating, Production, Storage, and Offloading Unit: A Case Study Using Variable Frequency Drives", *in 2022 IEEE Industry Applications Society Annual Meeting (IAS)*, pp. 1–6, 2022, doi:10.1109/IAS54023.2022.9939907.

[21] J. Pedra, L. Sainz, F. Corcoles, "Study of aggregate models for squirrel-cage induction motors", *IEEE Transactions on Power Systems*, vol. 20, no. 3, pp. 1519–1527, 2005, doi:10.1109/TPWRS.2005.852073.

[22] A. Sheldrake, *Handbook of Electrical Engineering: For Practitioners in the Oil, Gas and Petrochemical Industry.*, Wiley, 2016.

[23] L. F. da Rocha, D. I. Brandao, K. d. S. Medeiros, M. S. Dall'asta, T. B. Lazzarin, "Coordinated Decentralized Control of Dynamic Volt-Var Function in Oil and Gas Platform With Wind Power Generation", *IEEE Open Journal of Industry Applications*, vol. 4, pp. 269–278, 2023, doi:10.1109/OJIA.2023.3307299.

[24] S. G. Johansson, L. Liljestrand, F. Krogh, J. Karlstrand, J. Hanson, "AC Cable solutions for Offshore Wind Energy", *CITESEER Copenhagen Offshore Wind Conference*, pp. 1–10, 2005.

[25] J. Fang, H. Li, Y. Tang, F. Blaabjerg, "On the Inertia of Future More-Electronics Power Systems", *IEEE Journal of Emerging and Selected Topics in Power Electronics*, vol. 7, no. 4, pp. 2130–2146, 2019, doi:10.1109/JESTPE.2018.2877766.

[26] L. Ran, J. Bumby, P. Tavner, "Use of turbine inertia for power smoothing of wind turbines with a DFIG", *in 2004 11th International Conference on Harmonics and Quality of Power (IEEE Cat. No.04EX951)*, pp. 106–111, 2004, doi:10.1109/ICHQP.2004.1409337.

[27] T. Senjyu, R. Sakamoto, N. Urasaki, T. Funabashi, H. Fujita, H. Sekine, "Output power leveling of wind turbine Generator for all operating regions by pitch angle control", *IEEE Transactions on Energy Conversion*, vol. 21, no. 2, pp. 467–475, 2006, doi:10.1109/TEC.2006.874253.

[28] A. Uehara, A. Pratap, T. Goya, T. Senjyu, A. Yona, N. Urasaki, T. Funabashi, "A Coordinated Control Method to Smooth Wind Power Fluctuations of a PMSG-Based WECS", *IEEE Transac-*

tions on Energy Conversion, vol. 26, no. 2, pp. 550–558, 2011, doi:10.1109/TEC.2011.2107912.
[29] A. A. Adeyemo, E. Alves, F. Marra, D. Brandao, E. Tedeschi, "Suitability assessment of high-power energy storage technologies for offshore oil and gas platforms: A life cycle cost perspective", *Journal of Energy Storage*, vol. 61, p. 106643, 2023, doi:https://doi.org/10.1016/j.est.2023.106643.
[30] E. Alves, S. Sanchez, D. Brandao, E. Tedeschi, "Smart Load Management with Energy Storage for Power Quality Enhancement in Wind-Powered Oil and Gas Applications", *Energies*, vol. 12, no. 15, 2019, doi:10.3390/en12152985.
[31] Eaton, "Supercapacitor modules", Accessed on September 26, 2024, 2024, URL: https://www.eaton.com/content/dam/eaton/products/electronic-components/resources/data-sheet/eaton-xlhv-supercapacitor-module-data-sheet-elx1352-en.pdf.
[32] U. Akram, M. Nadarajah, R. Shah, F. Milano, "A review on rapid responsive energy storage technologies for frequency regulation in modern power systems", *Renewable and Sustainable Energy Reviews*, vol. 120, p. 109626, 2020, doi:https://doi.org/10.1016/j.rser.2019.109626.
[33] G. G. Njema, R. B. O. Ouma, J. K. Kibet, "A review on the recent advances in battery development and energy storage technologies", *Journal of Renewable Energy*, vol. 2024, no. 1, p. 2329261, 2024, doi:https://doi.org/10.1155/2024/2329261.
[34] A. Aghmadi, O. A. Mohammed, "Energy Storage Systems: Technologies and High-Power Applications", *Batteries*, vol. 10, no. 4, p. 141, 2024, doi:https://doi.org/10.3390/batteries10040141.
[35] R. B. Sepe, A. Steyerl, S. P. Bastien, "Lithium-ion supercapacitors for pulsed power applications", *in 2011 IEEE Energy Conversion Congress and Exposition*, pp. 1813–1818, 2011, doi:10.1109/ECCE.2011.6064005.

BIOGRAPHIES

Kassiane de S. Medeiros received the B.Sc. degree in electrical engineering, in 2012, and the M.Sc. degree in electrical engineering, in 2015, both from the Pontifical Catholic University of Minas Gerais, Belo Horizonte, Brazil. She is currently working toward the Ph.D. degree in electrical engineering with the Federal University of Minas Gerais, Belo Horizonte, Brazil. Her current research and technical interests include offshore energy, power-quality issues, and control strategies from power electronic converters.

João Marcus S. Callegari received the B.Sc. degree in electrical engineering from the Federal University of Viçosa, Brazil, in 2019, the M.Sc. degree in electrical engineering from the Federal Center of Technological Education of Minas Gerais, Brazil, in 2021, and the doctorate degree in electrical engineering at the Federal University of Minas Gerais, Brazil, in 2024. His current research and technical interests include the design and control of grid-connected multifunctional inverters, the reliability of power electronics-based systems, and AC microgrids. Mr. Callegari was the recipient of the President Bernardes Silver Medal in 2019 and the IEEE IAS CMD Student Thesis Contest 2022 (Non-PhD Category).

Ayotunde Adekunle Adeyemo was born in Ado-Ekiti, Nigeria, in 1991. He received the B.Sc. degree in electrical and electronic engineering from the University of Ibadan, Ibadan, Nigeria, in 2014, and the M.Sc. degree in electronic and electrical engineering from the University of Sheffield, Sheffield, U.K., in 2016. He is currently working toward the Ph.D. degree in electric power engineering with the Norwegian University of Science and Technology, Trondheim, Norway. From July 2012 to January 2013, he worked as an Electrical Intern with DeltaAfrik Engineering Limited (an oil and gas servicing company. During this period, he worked on cable sizing, generator sizing, switchgear design, and lighting design. From January 2018 to September 2018, he was with Sunhive Limited as an Electrical Engineer. During this period, he worked in a team of engineers to install and maintain hybrid energy systems comprising of solar photovoltaic panels, diesel generators, and battery energy storage. His research interests include power electronic converter control strategies for higher penetration of renewable energy in national grids, design, sizing, and control of battery energy storage systems for grid applications, power electronic converter control strategies for more electric aircraft, and mathematical optimization of hybrid energy systems.

Elisabetta Tedeschi received the M.Sc. (Hons.) degree in electrical engineering and the Ph.D. degree in industrial engineering from the University of Padua, Padua, Italy, in 2005 and 2009, respectively. From 2009 to 2011, she was a Postdoctoral Researcher with the Norwegian University of Science and Technology (NTNU), working on the grid integration of offshore renewable energies. She was a Researcher/Marie Curie Fellow with Tecnalia, Spain, from 2011 to 2013, where she worked as the Principal Investigator in the FP7-Sea2grid Project, related to the storage needs for the grid integration of wave energy converters. From 2013 to 2014, she was a Research Scientist with SINTEF Energy, and an Adjunct Associate Professor with NTNU. In 2014, she became a Full Professor within the offshore grid with NTNU. Since 2020, she has also been a Full Professor with the Department of Industrial Engineering, University of Trento, Trento, Italy. She has a core competence in the design and control of energy conversion and transmission and distribution systems, with a focus on offshore energy and power-quality issues. She has led and/or contributed to more than 15 national and international scientific projects and she has authored or coauthored two book chapters and more than 150 journals and conference papers in the field of marine energy and energy conversion systems.

Danilo I. Brandao received the doctorate degree in electrical engineering from the State University of Campinas (Unicamp), Brazil, in 2015. He was visiting positions at Colorado School of Mines (2009 and 2013), Università degli Studi di Padova (2014) and Norwegian University of Science and Technology (2018 and 2020). He is currently an assistant professor at Federal University of Minas Gerais (UFMG), Brazil. His main research interests are control of grid-tied converters and microgrids. He is a member of SOBRAEP.